Finite Elements in Analysis and Design 231 (2024) 104099

Contents lists available at ScienceDirect

Finite Elements in Analysis & Design

journal homepage: www.elsevier.com/locate/finel

NURBS-enhanced finite element method (NEFEM) on quadrilateral meshes

Mattia Montanari [a,*], Gian Maria Santi [b], Ruben Sevilla [c], Liverani Alfredo [b], Nik Petrinic [a]

[a] Department of Engineering Science, University of Oxford, United Kingdom
[b] Department of Industrial Engineering, University of Bologna, Italy
[c] Zienkiewicz Centre for Computational Engineering, Swansea University, United Kingdom

ARTICLE INFO

Keywords:
NEFEM
CAD integration
Quadrilateral elements

ABSTRACT

This paper formulates quadrilateral elements for the NURBS-enhanced finite element method (NEFEM). The objective is to extend the application of NEFEM to problems where the use of quadrilateral elements is preferred. By leveraging a mapping, between reference and physical spaces, that encapsulates the exact boundary representation of the domain, a tight integration with computer aided design (CAD) systems is achieved. The contribution of this work is an enhanced quadrilateral finite element that incorporates the exact CAD geometry purely from the boundary representation (B-rep) from CAD and without the need for a whole volume representation (V-rep) as a NURBS entity. Numerical examples involving heat transfer and linear elastic problems are used to numerically demonstrate the optimal convergence properties of the method under mesh refinement.

1. Introduction

This work is motivated by the ever-increasing desire to integrate geometry design and analysis into the computational engineering practice. This integration, possible by means of the isogeometric analysis (IGA) framework [1], is being halted by the need of volume-representations (V-rep) of the domain [2,3]. In-service computer aided design (CAD) packages only provide the boundary-representation (B-rep) of a domain, which is the information required by traditional mesh generators to obtain a finite element discretisation. This discrepancy is on of the main barriers between engineers and the advantages offered by IGA.

To offer a tight integration between geometry and analysis using the IGA framework, two avenues have been explored. The first one shifts from a B-rep to a V-rep paradigm by radically redefining CAD. For example, a B-rep of the unit cube comprises six surfaces connected along the edges, whereas its V-rep is a trivariate non-uniform rational B-spline (NURBS). The second alternative consists of devising algorithms to *automatically* convert a B-rep into a V-rep suitable for IGA. Both of these approaches are ongoing developments that face major obstacles. The former does not provide legacy with in-service CAD systems and it could overload graphic processors that need to render volumes rather than surfaces. The latter does not address the discrepancy between B-rep and V-rep, and therefore it defeats the original purpose.

An alternative to IGA is found in methods that are able to incorporate the B-rep into a finite element framework. The NURBS-enhanced finite element method (NEFEM) is one technique within this class. The main idea is to define a new type of finite element near the boundary of the domain. This new type of element accounts for the B-rep and proposes new strategies to define the

* Corresponding author.
E-mail address: exet3790@ox.ac.uk (M. Montanari).

https://doi.org/10.1016/j.finel.2023.104099
Received 26 June 2023; Received in revised form 23 November 2023; Accepted 28 November 2023
Available online 21 December 2023

functional approximation and to perform the numerical integration in those elements, whereas standard FEM is used in the rest of the domain. NEFEM has been applied to the numerical solution of heat transfer, electromagnetic and flow problems in two and three dimensions [4–6]. However, NEFEM has only been devised to work on triangular and tetrahedral meshes. This is a limitation to its applicability since it makes it unassailable to those applications, such as explicit nonlinear solid mechanics, for which quadrilateral and hexahedral elements are preferred.

This work introduces quadrilateral NURBS-enhanced finite elements and provides the following contributions:

- Confirms that NEFEM can integrate finite element analysis with in-service CAD tools.
- Represents curved boundaries on quadrilateral elements exactly as CAD does.
- Extends the use of NEFEM where the use of quadrilateral elements is preferred.

The potential that NEFEM offers is twofold: (i) design cost reduction brought by integration between CAD and FEM, and (ii) higher accuracy though exact CAD boundary representation. This work extends the range of applications that can benefit from NEFEM, particularly solid mechanics and boundary layers in the simulation of high speed compressible flows, since quadrilateral and hexahedral elements are often preferred.

2. Background

Since it was first formulated by Hughes et al. [1], the integration of geometry and analysis via IGA remains to a large extent theoretical; the scientific community however is actively looking for a robust solution to better integrate CAD and analysis. The difficulties encountered by the IGA community when creating trivariate NURBS models motivated the appearance of other methods that provide a coupling of geometry and analysis by only employing the B-rep that is available in modern CAD packages. The NEFEM rationale is one of the techniques capable of producing such coupling but its application and potential remains largely unexplored when compared to IGA.

This section reviews the current difficulties encountered by IGA, due to the need of a V-rep. The current state of the art of NEFEM is also reviewed, highlighting the developments required to devise a solution of practical interest to solid mechanics. Finally, a brief comparison between FEM, IGA and NEFEM is presented.

2.1. Boundary and volume representations

Several authors report that the gap between CAD and analysis exists because their development followed different paths [2,7,8]. The CAD technology consolidated in the 1990s, when computing power was extremely limited. As processing units improved, CAD moved from two-dimensional (2D) to three-dimensional (3D) representations, but always relying on B-reps to model solids — and still does today. CAD tools prefer B-reps to V-reps because they offer better computational performance and are mathematically easier to handle. For example, to draw a hollow shape, B-reps naturally extrude a profile, whereas V-reps would need to add trimming or subdivision techniques. The idea of using V-rep for CAD models is however the requirement to integrate IGA in engineering practice [9–11].

To equip CAD with V-rep, recent works have studied feasibility and accuracy [12–15] and revealed major challenges when working with complex geometries. The main difficulty is to retain orthogonal basis after (local) refinement. Locally refined B-splines [8] have recently been proved to give satisfactory results for 2D problems. This technology however seems to imply a major disruption into existing CAD systems, and so do other methods using script-based approaches [16–18]. In either case, the workflow appears cumbersome as it departs significantly from modern engineering practice. Other cases, such as [19] are limited to shell structures.

Approaches offering legacy with modern CAD-analysis workflows exist and they aim to reconstruct V-reps out of B-reps. The main argument supporting this approach is that by harnessing B-reps there would be no need to modify the current practice within the CAD community and its standards. However, in practice, generating a V-rep out of a B-rep for arbitrary shapes, even in 2D, is not a trivial task. This is due to the need of optimisation techniques and quadrilateral/hexahedral mesh generation [20]. For 3D models the complexity is remarkably higher [21] and the quality of the resulting mesh is not as good as what in-service FEA tools usually produce. Tools that do produce high-quality meshes tend to apply Bézier extraction recursively [22–25], but the resulting elements do not have the larger support that brings many of the benefits of the IGA [1]. Techniques that avoid Bézier extraction showed that even primitive shapes require advanced algorithms [26–28] and in some occasions these techniques are restricted to thin structures only [29]. A recent work [30] claimed a major leap forward but its applicability is limited to shapes mappable unit cubes — confirming the outcome of [17].

Recent works can be found with promising techniques to form a bijective parametrisation of solid domains [31], but overall, constructing a V-rep out of B-rep is an approach that shows three evident shortfalls:

1. From a mathematical standpoint it is a difficult, and possibly ill-posed, problem that requires mapping a (non-convex) surface into a volume.
2. Even if such mapping exists, the resulting volume representation must meet the quality requirements of FE mesh. In particular, the parametrisation of the volume must ensure the smoothness required to guarantee convergence under h and p refinement.
3. The bespoke V-rep used for analysis is not the same mathematical construct generated within CAD systems, leaving little hope for a seamless integration between modern CAD systems and analysis.

The reader is referred to the extensive review published by Perduta et al. on the integration challenges of classic IGA with in-service CAD systems [3].

Table 1
Summary of systematic review comparing FEM, IGA and NEFEM.

	FEM	IGA	NEFEM
V-rep:	Polynomials	NURBS	Hybrid
B-rep:	Approx.	Exact[a]	Exact
Lowest order of shape functions:	1st	2nd	1st
Numerical integration:	Exact/Approx.	Approx.	Approx.
Essential BC's at the nodes:	Exact	Approx	Exact

[a] Theoretical result, in practice this might not be achieved with modern CAD systems.

2.2. NURBS-enhanced finite element method

Another viable approach for CAD-analysis integration is the NURBS-enhanced finite element method (NEFEM) [4]. This technique is designed to seamlessly integrate the B-rep from CAD with a standard FEM mesh to provide an exact discretisation of the geometry. The fact that NEFEM uses the B-rep as given by modern CAD systems is the key advantage and enables CAD-analysis integration. NEFEM does requires only the B-rep without any refinements or editing. Unlike IGA, NEFEM is designed to work with standard CAD file such as IGES or STEP. Somewhat similar to the blended elements present in [32], but using classic FEM meshes instead of NURBS to represent volumes.

NEFEM was originally proposed in two dimensions and applied to heat transfer and electromagnetic problems using a standard FEM and a discontinuous Galerkin (DG) formulation, respectively [5]. The extension to three dimensional problems and to other fields such as compressible flow simulations was introduced in [4,5]. The use of NEFEM for fluids and solid mechanics has been recently proposed in the context of the hybridisable DG method, with particular emphasis on degree adaptive strategies that are able to maintain the exact B-rep during the adaptivity process [6,33]. The results show that incorporating the exact B-rep into the FE simulations lead to important gain on accuracy when compared to traditional isoparametric elements due to two main facts. First, NEFEM completely removes any geometric error introduced by the isoparametric representation of the boundary. Second, NEFEM removes the non-physical artefacts introduced by a piecewise representation of the boundary. These artefacts include non-physical entropy production in fluid flow simulations and concentration of stresses in solid mechanics applications.

The benefits shown by NEFEM have prompted its incorporation in other grid-based numerical methodologies such as finite volumes [34], space–time elements [35,36] and interface problems [37]. The results show that the benefits of such a tight integration between geometry and analysis go beyond the particular use of standard continuous or discontinuous finite elements. However, one difficulty preventing the widespread adoption of this technique is the mesh generation process. To fully exploit the benefits of NEFEM, a mesh technology that is capable of generating valid meshes that encapsulate the B-rep is required. For simple geometries the use of standard mesh generators is a feasible option but for complex geometries with multiscale features specifically designed techniques are required.

To date, the NEFEM mesh generation problem has only been solved in two dimensions and using triangular elements [38]. This difficulty lies in generating elements that preserve a positive Jacobian when curving the boundary a B-rep. This has encouraged researchers to extend the NEFEM rationale to methodologies that do not require a boundary fitted mesh. These extensions include the combination of NEFEM in with immersed FEs [39], boundary elements [40] and mesh-free methods [41]. The current limitation on the mesh generation for NEFEM halts the scope of this work which is limited to two-dimensional domains.

The original NEFEM formulation is however restricted to triangular and tetrahedral elements. The lack of quadrilateral and hexahedral formulations is a limitation to the space of available shape functions, hence a limit to the accuracy of the method. This is of particular importance in solid mechanics, where quadrilateral and hexahedral elements are commonly favoured [42] but their NURBS-enrichment has been limited to interfaces in 2D problems only [43]. The simulation of high speed compressible flows can also benefit from an extension of NEFEM to quadrilateral and hexahedral meshes its use in boundary layers.

2.3. Comparison between FEM, IGA and NEFEM

This section discusses the main differences between the classical FEM [42], IGA [9] and NEFEM [5]. These differences are summarised in Table 1.

Regarding the volume representation of the computational domain, FEM uses a piecewise polynomial description of the geometry. The computational domain is subdivided into elements and the boundary of the computational domain is approximated with piecewise polynomials of the desired degree that, in general, do not represent the boundary exactly. IGA uses NURBS to represent the volume under consideration and represents boundary exactly. However, as discussed in Section 2.1, its V-rep is not compatible with modern CAD systems and in practice creates a gap between CAD and analysis: the former provides a B-rep, while the latter needs a different monolithic representation used in IGA. With NEFEM, the volume is represented using a hybrid approach. Those elements sharing a face or an edge with the boundary inherit the CAD B-rep, whereas the rest of the elements follow an isoparametric description. For boundary elements, NEFEM directly uses NURBS B-rep, without modification, meaning that the boundary matches exactly the description provided by modern CAD systems.

When considering the application of finite elements to problems in the field of solid mechanics, it is important to note that linear elements are still the predominant and preferred option to be used in industrial applications. With IGA, the use of linear basis

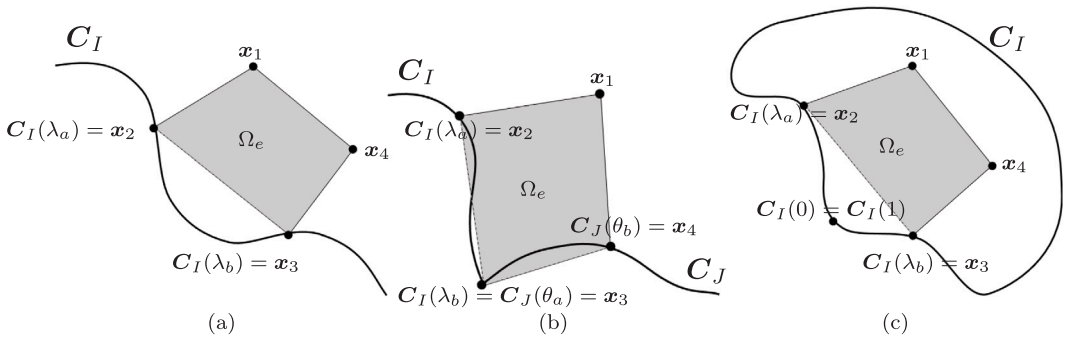

Fig. 1. Examples of feasible NEFEM elements. (a) An element with an edge given by a NURBS curve. (b) An element with two edges given by two different NURBS curves. (c) An element with an edge given by a NURBS closed curve.

functions reduces to the standard FEM. However, with NEFEM it is possible to use a linear approximation for the solution whilst maintaining the exact B-rep. This is due to the decoupling of the two concepts tightly coupled in isoparametric or isogeometric methods, namely the geometric and solution representation.

For all the methods considered here, it is necessary to approximate the integrals of the weak formulation by means of numerical quadratures. With standard FEM, it is possible to compute the integrals exactly in many situations. For instance, the terms of the mass matrix can always be integrated exactly using a numerical quadrature and, for cases where the Jacobian of the isoparametric mapping is constant, the entries of the stiffness matrix can also be exactly computed. However, when the Jacobian of the isoparametric mapping is not constant the integrals can only be computed approximately [44]. For IGA and NEFEM, the integrals are always computed approximately due to the rational nature of NURBS [45]. It is worth noting that complex CAD models used in industrial applications contain a large number of B-splines and rational surfaces appear in limited occasions, when containing conics for instance. This means that in many occasions, it is also possible to compute exactly the integrals appearing in a NEFEM formulation.

Regarding the imposition of boundary conditions, natural and essential conditions are mainly of interest in solid mechanics. Natural boundary conditions are handled equally in the three methods considered, whereas important differences arise when considering essential boundary conditions. In FEM and NEFEM essential boundary conditions can be exactly imposed at the nodes following the standard practice of reducing the system of linear equations. However, with IGA the imposition of non-homogeneous essential boundary conditions is not trivial and not exact at the nodes [46].

3. NEFEM formulation for quadrilaterals

This section presents a novel quadrilateral formulation for NEFEM. The approach presented is general and can be extended to high order approximations.

3.1. Pre-processing

Given a domain Ω, described by the B-rep, $\mathcal{B}$, of the boundary $\partial\Omega$ and a standard finite element mesh $\mathcal{M}$, given by a disjoint set quadrilateral elements, $\mathcal{E}$, and the nodal coordinates, $\mathcal{N}$. This section describes the pre-process that is required to obtain the data structures employed in a NEFEM solver.

The first step consists of reading the set of curves, $\mathcal{C}$, within the B-rep, $\mathcal{B}$. More precisely, NEFEM requires the set of control points and weights and the knot vector for each NURBS curve $C_I \in \mathcal{C}$. In this work, this information is extracted from a standard CAD file (e.g. IGES or STEP) using the open source OpenCascade library.

The second step consists of identifying the elements with at least one edge on $\partial\Omega$ and, for each edge on the boundary, the associated NURBS curve. It is worth noting that some mesh generators directly output this information, so that boundary conditions can be assigned to a set of edges or nodes that belong to a NURBS curve. If this information is not available within the given finite element mesh, it can be easily computed at this stage using a NURBS point projection algorithm.

At this stage, the set of elements $\mathcal{E}$ is partitioned into elements with at least one edge on the boundary, $\mathcal{E}^b$ and interior elements $\mathcal{E}^i$, with $\mathcal{E}^b \cup \mathcal{E}^i = \mathcal{E}$ and $\mathcal{E}^b \cap \mathcal{E}^i = \emptyset$. For each element $\Omega_e \in \mathcal{E}^b$, a list of boundary edges and the associated NURBS is readily available.

In a traditional low-order FEM solver, the elements are simply defined by their vertices. In NEFEM, this definition is maintained for all elements in $\mathcal{E}^i$, but a NURBS-enhanced definition is introduced for those elements with at least one edge on the boundary. An element $\Omega_e \in \mathcal{E}^b$ is defined by replacing the original straight edges on $\partial\Omega$ by the trimmed NURBS that connects the two nodes on $\partial\Omega$. Fig. 1 shows three examples of quadrilateral elements with at least one node on $\partial\Omega$.

The first example, in Fig. 1(a), shows an element with nodes $\boldsymbol{x}_2$ and $\boldsymbol{x}_3$ on the NURBS curve C_I. The parametric coordinates of the nodes are λ_a and λ_b respectively. In this example, the original element Ω_e as shown in the Figure would be enhanced by replacing

the straight edge connecting nodes $\boldsymbol{x}_2$ and $\boldsymbol{x}_3$ by the NURBS curve C_I trimmed to the interval $[\lambda_a, \lambda_b]$. The second example, in Fig. 1(b), depicts an element with two edges defined by two different NURBS curves, namely the edge connecting nodes $\boldsymbol{x}_2$ and $\boldsymbol{x}_3$ on the NURBS curve C_I and the edge connecting nodes $\boldsymbol{x}_3$ and $\boldsymbol{x}_4$ on the NURBS curve C_J. To equip this element with a NEFEM rationale, each edge will be defined by a trimmed NURBS curve. Finally, the third example, in Fig. 1(c), shows a situation where the NURBS curve defining the boundary is a closed curved, so $\boldsymbol{C}_I(0) = \boldsymbol{C}_I(1)$ and the edge connecting the nodes $\boldsymbol{x}_2$ and $\boldsymbol{x}_3$ traverses the periodic point. In this case, the curved edge will be defined as the collection of two trimmed curves, namely the curve $\boldsymbol{C}_I$ trimmed to $[\lambda_a, 1]$ and the same curve $\boldsymbol{C}_I$ trimmed to $[0, \lambda_b]$. It is worth noting that the last example assumes, without loss of generality, that the parametric space of the curve $\boldsymbol{C}_I$ is $[0, 1]$.

3.2. Basis functions

For those elements with no edges on the boundary, NEFEM uses a standard FE formulation. This means that the approximation of the solution u, denoted by u_h, is defined in a reference element, with local coordinates ξ and η. For a bi-linear quadrilateral the approximation is defined as

$$u_h(\xi, \eta) = \sum_{j=1}^{4} N_j(\xi, \eta) u_j, \tag{1}$$

where u_j and N_j are the nodal value and the bi-linear shape function associated to node (ξ_j, η_j).

For elements with at least one edge on the NURBS boundary, the traditional approach followed in NEFEM consists of defining the polynomial basis directly in the physical space, with Cartesian coordinates x and y. In this work, this traditional approach is not followed. Instead, the approximation traditionally used in FEM solvers is favoured, meaning that the same approximation is employed for all the elements.

To justify the choice made for the basis functions employed in NEFEM elements, it is worth recalling the motivation for selecting a different approximation in the existing implementations of NEFEM. First, it is important to note that all NEFEM approaches proposed in boundary fitted meshes are only designed to work on triangular and tetrahedral meshes. In this scenario elements with no edges on the boundary are triangular elements with straight edges and therefore they always have a constant Jacobian. This property implies that defining the polynomial basis in the physical element or in the reference element is equivalent because the isoparametric mapping is always affine. From a computational point of view, it is clearly preferred to define the basis in a reference element. However, for NEFEM elements, the definition of the basis in a parametric space or in the physical space is not equivalent as the mapping cannot be affine and at the same time account for the exact B-rep. For consistency, the original NEFEM formulation in triangles and tetrahedra proposed the definition of the basis functions for NEFEM elements in the physical space. With this approach, the resulting methodology was able to provide reproducibility of polynomials of any degree in the physical space [44].

In this work the interest is in extending the NEFEM rationale to quadrilateral elements. Even for standard FEM quadrilateral elements the mapping between the reference element and the physical element is only affine if the opposite edges of the quadrilateral are parallel, so in general the mapping is not affine. This implies that in standard FEM the basis functions are polynomials in the reference element but not necessarily in the physical space. For this reason, in this work there is no benefit on defining the basis functions for NEFEM elements in the physical space and they are defined always in the reference element, for both FEM and NEFEM elements.

It is worth mentioning that it is possible to define the shape functions for all elements in the physical space. However, this option is not advocated here as it will increase the cost of computing the elemental matrices. In the original NEFEM approach for triangles and tetrahedra this was not an issue because the shape functions in the physical space were only generated for a very small percentage of the total number of elements, only for the elements with at least one edge or face on the boundary.

3.3. Mapping between local and physical coordinates

For FEM elements, with no edges on a boundary defined by a NURBS curve, the mapping from the reference element $[0, 1]^2$ to the physical element is the classical isoparametric mapping, given by

$$\boldsymbol{\psi}(\xi, \eta) = \sum_{k=1}^{4} N_k(\xi, \eta) \boldsymbol{x}_k, \tag{2}$$

where N_k is the bi-linear shape function associated to node (ξ_k, η_k).

The new mapping considered by NEFEM quadrilateral elements is the patch due to Coons who introduced, in [47], an injective and continuously differentiable function able to parametrise the surface enclosed by four curves.

The mapping from the reference element $[0, 1]^2$ to a quadrilateral NEFEM element Ω_e is written as

$$\boldsymbol{\psi}(\xi, \eta) = \sum_{i=1}^{2} \widetilde{N}_i(\eta) \boldsymbol{C}_i(\xi) + \sum_{j=1}^{2} \widetilde{N}_j(\xi) \boldsymbol{D}_j(\eta) - \sum_{k=1}^{4} N_k(\xi, \eta) \boldsymbol{x}_k, \tag{3}$$

where $\{\widetilde{N}\}_{l=1,2}$ denote the linear shape functions in the one dimensional reference element $[0, 1]$. The parametric curves $\{\boldsymbol{C}_l\}_{l=1,2}$ describe the edges connecting nodes $\boldsymbol{x}_4$ and $\boldsymbol{x}_3$ and nodes $\boldsymbol{x}_1$ and $\boldsymbol{x}_2$, respectively. Similarly, the parametric curves $\{\boldsymbol{D}_l\}_{l=1,2}$ describe the edges connecting nodes $\boldsymbol{x}_2$ and $\boldsymbol{x}_3$ and nodes $\boldsymbol{x}_1$ and $\boldsymbol{x}_4$, respectively.

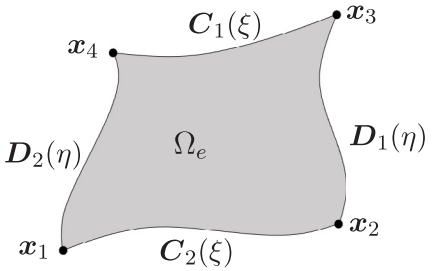

Fig. 2. Illustration of the parametrisation of a curved NEFEM element using the mapping defined in Eq. (3).

The parametrisation of a curved NEFEM quadrilateral element induced by the mapping of Eq. (3) is illustrated in Fig. 2. It is worth noting that for the majority of NEFEM elements, not all the faces are curved, as illustrated in Fig. 1. When one of the edges of a NEFEM quadrilateral element is straight (i.e. not on the boundary), the parametrisation is simply given by the two nodes that connect this edge. For instance, if the edge connecting the nodes $\boldsymbol{x}_2$ and $\boldsymbol{x}_3$ is a straight edge, the parametrisation $\boldsymbol{D}_1$ is simply

$$\boldsymbol{D}_1(\eta) = \eta \boldsymbol{x}_2 + (1-\eta)\boldsymbol{x}_3. \tag{4}$$

3.3.1. Numerical integration

The weak form of the problem at hand requires to compute numerically integrals over elements and, when natural boundary conditions are involved, integrals over boundary edges.

Let us consider the computation of a generic entry of a stiffness matrix, namely

$$K^e_{ij} = \int_{\Omega_e} \boldsymbol{\nabla}_x N_i \cdot \boldsymbol{\nabla}_x N_j \, dx dy = \int_0^1 \int_0^1 \left(\boldsymbol{J}_\psi^{-1} \boldsymbol{\nabla}_\xi N_i \right) \cdot \left(\boldsymbol{J}_\psi^{-1} \boldsymbol{\nabla}_\xi N_j \right) |\boldsymbol{J}_\psi| d\xi\eta, \tag{5}$$

where $\boldsymbol{\nabla}_x$ denotes the gradient with respect to the physical coordinates, $\boldsymbol{\nabla}_\xi$ is the gradient with respect to the local coordinates and the Jacobian of the mapping between local and physical coordinates is given by

$$\boldsymbol{J}_\psi = \begin{bmatrix} \dfrac{\partial \psi_1}{\partial \xi} & \dfrac{\partial \psi_2}{\partial \xi} \\ \dfrac{\partial \psi_1}{\partial \eta} & \dfrac{\partial \psi_2}{\partial \eta} \end{bmatrix} \tag{6}$$

The integrals cannot be exactly computed in general, even for standard finite elements due to the appearance of the inverse of Jacobian of the mapping. In this work, they are evaluated using Gaussian quadratures defined in the reference element $[0, 1]$.

The components of the Jacobian for a FEM element only require the computation of the derivatives of the shape functions in the reference element. From a computational point of view, these derivatives are precomputed at the Gauss integration points.

For a NEFEM element, the components of the Jacobian are computed as

$$\frac{\partial \boldsymbol{\psi}}{\partial \xi} = \sum_{i=1}^{2} \widetilde{N}_i(\eta) \boldsymbol{C}_i'(\xi) + \boldsymbol{D}_1(\eta) - \boldsymbol{D}_2(\eta) - \sum_{k=1}^{4} \frac{\partial N_k}{\partial \xi} \boldsymbol{x}_k, \tag{7a}$$

$$\frac{\partial \boldsymbol{\psi}}{\partial \eta} = \boldsymbol{C}_1(\xi) - \boldsymbol{C}_2(\xi) + \sum_{j=1}^{2} \widetilde{N}_j(\xi) \boldsymbol{D}_j'(\eta) - \sum_{k=1}^{4} \frac{\partial N_k}{\partial \eta} \boldsymbol{x}_k, \tag{7b}$$

which requires evaluating the derivatives of the curves parametrising the boundary of the element.

The computation of the boundary integrals for quadrilateral NEFEM elements involves the computation of integrals over trimmed NURBS, which is exactly the same as when triangular elements are used. In [44] the authors explore different alternatives to compute such integrals and conclude that Gauss quadratures are the most attractive option as they are able to provide the maximum accuracy for a given number of integration points.

The sufficient number of integration points for an accurate result is set by a rule of thumb. For bilinear shape functions, NEFEM elements employ three Gauss points in each parametric coordinate, whereas FEM use only two Gauss points. Numerical evidence will show that this rule of thumb is an effective compromise to limit the error due to numerical integration, while keeping the computational overhead extremely low compared to the classic FEM formulation.

A mesh involving highly distorted elements would, in principle, require a higher number of Gauss points to retain accuracy, however in such hypothetical scenario a stronger constrain would halt NEFEM. The mapping introduce in this work is not automatically guaranteed to be a valid: the necessary condition is that the Jacobian in Eq. (6) is positive in the domain. This condition should be verified at runtime simply by checking the Jacobian at the Gauss points is valid and, if necessary, a suitable mitigation strategy should be used. For example, depending on the application, element erosion or a local mesh refinement can quickly solve this issue.

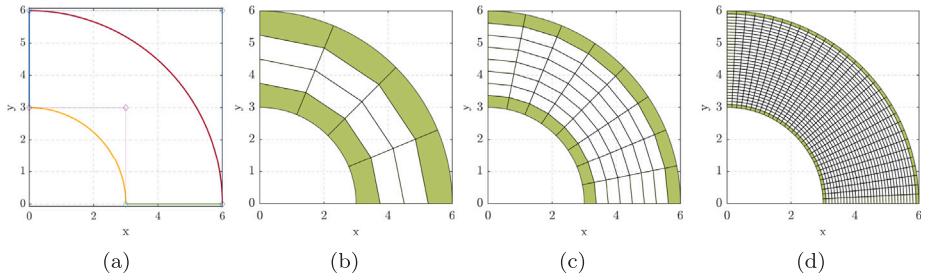

Fig. 3. (a) The geometry of the circular annulus showing the control points of the four different NURBS describing the boundary. Meshes with (b) 16, (c) 64 and (d) 1024 elements are displayed and NEFEM elements are highlighted in green.

Remark 1. NURBS curves defining the boundary of the element might contain internal breakpoints (i.e. points where the NURBS definition changes). In such case there is no need to subdivide or re-map elements for the numerical integration: the volume is always integrated from a tensor product of one 1D quadrature per edge. This is avoids the need for remapping or element subdivision.

4. Numerical results

This section presents numerical results involving heat transfer and linear elasticity problems. The objective is to numerically demonstrate the optimal convergence properties of the proposed approach and to compare its accuracy against classical isoparametric bi-linear elements. To this end, examples with known analytical solutions are first considered and the error in the $\mathcal{L}^2(\Omega)$ norm is used to measure the accuracy.

4.1. Heat transfer

This first test considers a heat transfer problem modelled by the Poisson equation, namely

$$\begin{cases} -\Delta u = f & \text{in } \Omega \\ u = u_D & \text{on } \Gamma_D \\ \nabla u \cdot \boldsymbol{n} = g_N & \text{on } \Gamma_N, \end{cases} \tag{8}$$

where u is the temperature field, f is the external source, u_D is the imposed temperature on the Dirichlet boundary Γ_D, g_N is the imposed heat flux on the Neumann boundary Γ_N and $\boldsymbol{n}$ is the outward unit normal vector to the boundary.

The external heat source and the boundary conditions are selected such that the analytical temperature is known and given by

$$u(x, y) = x\cos(y) + y\sin(x). \tag{9}$$

The computational domain corresponds to a quarter of a circular annulus, with internal radius equal to three and external radius equal to six, as depicted in Fig. 3(a). The boundary is given by four NURBS curves. Two curves are just linear B-splines whereas the other two are NURBS exactly representing the two concentric circles. Dirichlet boundary conditions are imposed on the polygonal part of the boundary and Neumann boundary conditions on the curved part of the boundary.

Fig. 3 also shows three successively refined meshes with 16, 64 and 1024 quadrilateral elements. In green are depicted NEFEM elements, whereas the in white are standard FEM elements. It is worth noting that when labelling NEFEM and FEM elements, no distinction has been made about the different nature of the NURBS curves describing the boundary. If desired, it is easy to check if a boundary curve is a straight line and flag the elements with at least one edge on this curve as FEM elements.

The temperature field computed with standard isoparametric bi-linear elements and with the proposed NEFEM approach are displayed in Fig. 4. The top figures show the solution computed with FEM and the bottom figures the solution employing NEFEM. As expected, there are some small differences in the isolines that can be observed when coarser meshes are used. The differences are less evident when the mesh is refined. It is worth noting that with NEFEM the boundary of the computational domain is always the one given by the exact B-rep, whereas with FEM an important discrepancy between the exact boundary and the computational boundary is observed, specially for coarse meshes.

Fig. 5 shows the convergence of the $\mathcal{L}^2(\Omega)$ error as a function of the minimum element size. First, the results demonstrate the optimal (i.e. quadratic) convergence of both FEM and NEFEM. This is expected as both methods employ a bi-linear approximation of the solution in the reference element. In addition, it is important to note that NEFEM offers an improvement for all levels of mesh refinement, and not only for coarse meshes.

To further illustrate the benefits of the proposed approach, Table 2 summarises the results, including the number of degrees of freedom of each simulation, the error of FEM and NEFEM computations and the relative difference between the FEM and NEFEM $\mathcal{L}^2(\Omega)$ errors.

The results show that NEFEM is between 20% and 30% more accurate than FEM using the same number of degrees of freedom and bi-linear shape functions. Contrary to the belief that an accurate geometric representation is only relevant when using high

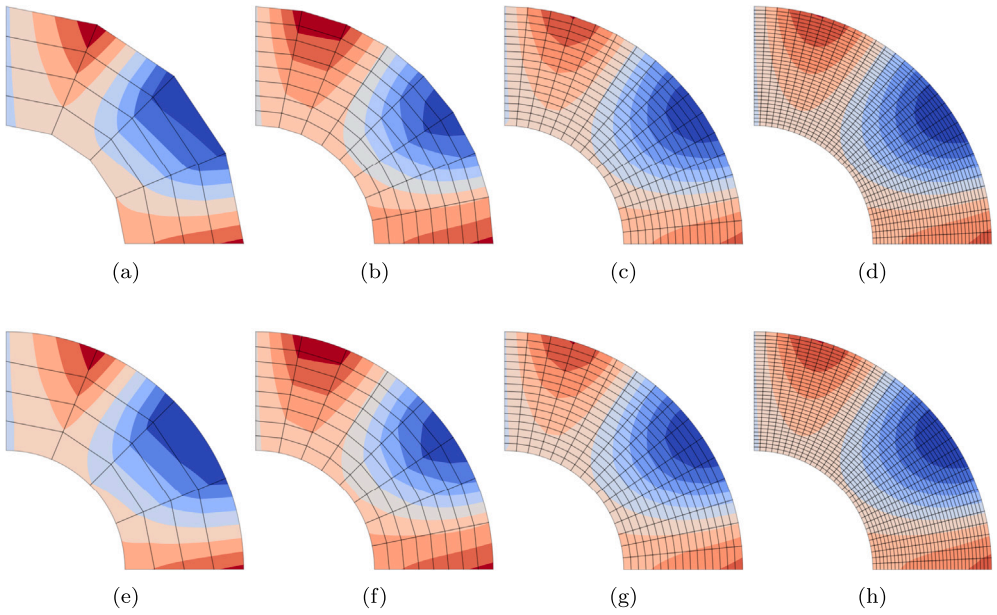

Fig. 4. Heat transfer problem: computed temperature field with FEM (top figures) and NEFEM (bottom figures) on four successively refined meshes.

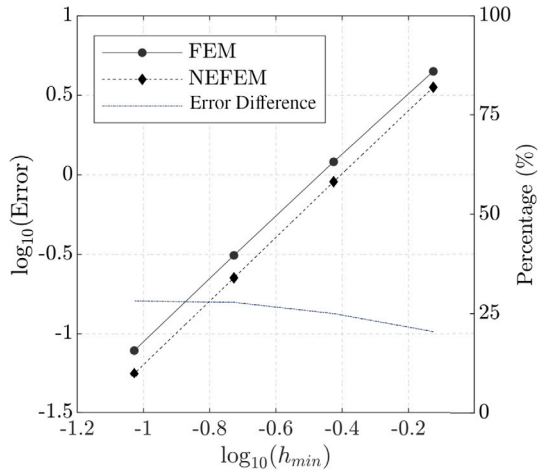

Fig. 5. Heat transfer problem: $\mathcal{L}^2(\Omega)$ error for FEM and NEFEM as a function of the minimum element size.

Table 2
Heat transfer problem: $\mathcal{L}^2(\Omega)$ error for FEM and NEFEM and their relative difference as a percentage.

$h_{\min}$	dof	Error		
		FEM	NEFEM	Difference
0.750	16	4.47×10^{0}	3.55×10^{0}	20.5%
0.375	81	1.21×10^{0}	9.05×10^{-1}	25.1%
0.190	289	3.11×10^{-1}	2.25×10^{-1}	27.9%
0.095	1089	7.83×10^{-2}	5.62×10^{-2}	28.2%

Table 3
Linear elastic problem: $\mathcal{L}^2(\Omega)$ error for FEM and NEFEM and their relative difference as a percentage.

$h_{\min}$	dof	Error		
		FEM	NEFEM	Difference
0.750	50	8.64×10^{-2}	4.56×10^{-2}	47.2%
0.375	182	1.54×10^{-2}	8.56×10^{-3}	44.3%
0.190	578	2.71×10^{-3}	1.59×10^{-3}	41.1%
0.095	2178	4.75×10^{-4}	2.99×10^{-4}	37.2%

order elements and coarse meshes, this examples shows that even when fine meshes of low order elements are used, the benefits of NEFEM are substantial.

It is worth noting that despite NEFEM elements require more integration points, when the mesh is refined, the number of NEFEM elements is a very small portion of the total number of elements. For instance, in the fourth mesh considered in this study, with 1024 element, there are only 64 NEFEM elements. In addition, to accurately compute the integrals of the weak form in a NEFEM quadrilateral element, it is only necessary to increase the number of integration points in the direction associated to the boundary edge, and not in the direction associated to interior edges. This means that the extra cost induced by NEFEM is negligible.

4.2. Linear elasticity

The second example considers a linear elastic problem, governed by the boundary value problem

$$\begin{cases} -\boldsymbol{\nabla}\cdot\boldsymbol{\sigma} = \boldsymbol{f} & \text{in } \Omega, \\ \boldsymbol{u} = \boldsymbol{u}_D & \text{on } \Gamma_D, \\ \boldsymbol{n}\cdot\boldsymbol{\sigma} = \boldsymbol{g}_N & \text{on } \Gamma_N, \end{cases} \tag{10}$$

where $\boldsymbol{u}$ is the displacement field, $\boldsymbol{\sigma}$ is the Cauchy stress tensor, $\boldsymbol{f}$ denotes a volumetric external force, $\boldsymbol{u}_D$ is the imposed displacement on the Dirichlet boundary and $\boldsymbol{g}_N$ is the imposed traction vector on the Neumann boundary.

The test considered is the so-called Lamé problem. It consists of a thick-walled cylinder of infinite length subject to a uniform internal and external pressure. The solution is computed in a quarter of the domain using the symmetry of the problem, leading to the same domain as the one considered for the heat transfer problem, shown in Fig. 3. There are no volumetric forces applied and the exact solution can be written, in polar coordinates, as

$$u(r) = C_1\, r + \frac{C_2}{r}, \tag{11}$$

where

$$C_1 = \frac{\nu - 1}{\nu\, E}\,\frac{p_e r_e^2 - p_i r_i^2}{r_e^2 - r_i^2}, \qquad C_2 = \frac{\nu + 1}{\nu\, E}(p_e - p_i)\frac{r_e^2 r_i^2}{r_e^2 - r_i^2}. \tag{12}$$

In the above expressions, $r = \sqrt{x^2 + y^2}$, r_e and r_i and the external and internal radii of the annulus respectively, $p_e = 0.5$ MPa and $p_i = 1.5$ MPa and the external and internal pressure applied respectively, $\nu = 0.3$ is the Poisson's ration and $E = 1$ MPa is the Young modulus.

In this example, the meshes considered are also the same meshes used in the previous example. This setting is used to evaluate the potential advantages of NEFEM in a solid mechanics problem using the same discretisations employed for the heat transfer problem.

The displacement field computed with standard isoparametric bi-linear elements and with the proposed NEFEM approach are displayed in Fig. 6. The top figures show the solution computed with FEM and the bottom figures the solution employing NEFEM. A visual comparison of the results reveals that NEFEM presents the boundary exactly.

Fig. 7 shows the convergence of the $\mathcal{L}^2(\Omega)$ error as a function of the minimum element size. The results show the optimal convergence of both FEM and NEFEM approaches. Furthermore, the extra accuracy of NEFEM can be clearly observed. In fact, the results in the figure indicate that NEFEM offer greater advantages for the elastic problem, when compared to the results presented for the heat transfer problem.

Table 3 summarises the results, including the number of degrees of freedom of each simulation, the error of FEM and NEFEM computations and the relative difference between the FEM and NEFEM $\mathcal{L}^2(\Omega)$ errors.

The comparison shows that NEFEM is between 35% and 50% more accurate than FEM. The extra accuracy provided by NEFEM is substantially higher than in the previous example, showing the potential of the proposed approach in linear elastic problems.

4.3. CAD integration

In this section two applications considering more complex CAD geometries are considered to further evaluate the potential and benefits of the proposed quadrilateral NEFEM formulation.

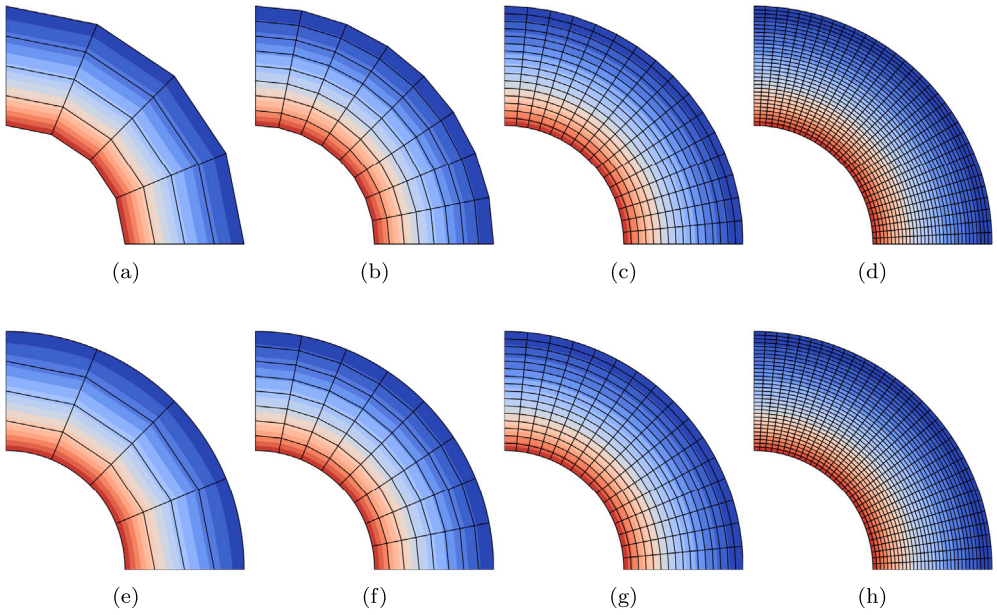

Fig. 6. Linear elastic problem: computed displacement field with FEM (top figures) and NEFEM (bottom figures) on four successively refined meshes.

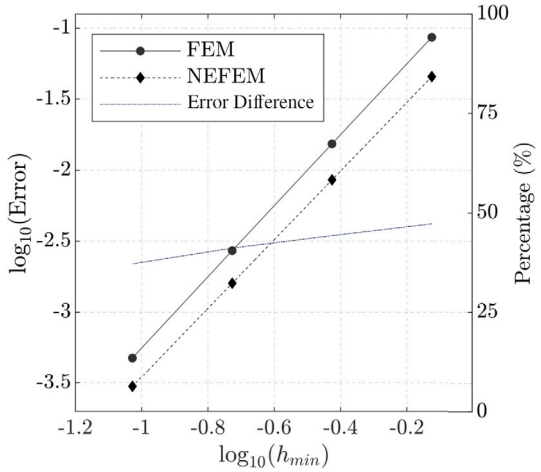

Fig. 7. Linear elastic problem: $\mathcal{L}^2(\Omega)$ error for FEM and NEFEM as a function of the minimum element size.

The first example considers the CAD model of a fir tree root blade commonly found in turbine engines. This is imported, pre-processed and analysed following the steps outlined in Section 3. A detailed view of the geometry, together with the computed displacement, is shown in Fig. 8. This figure also shows a detailed view of the discretisation used near the boundary, highlighting the elements where the NEFEM formulation is used. In this example, the preprocess has been enhanced to ensure that the elements in contact with the polygonal part of the boundary are considered as FEM elements.

Homogeneous Dirichlet boundary conditions are applied on the lower part of the geometry and an upward force is applied on the teeth of the discs representing the centrifugal forces action on the turbine blades. As no analytical solution is available for this problem, a reference solution, computed using bi-quadratic finite elements.

The mesh contains 8503 quadrilateral elements and the preprocess stage partitions the mesh into 606 NEFEM elements and 7897 FEM elements. The results indicate that using NEFEM the error can be reduced by almost 13% compared to the results obtained with standard bi-linear quadrilaterals. It is worth noting that in this example, the large majority of the mesh is made of standard FEM elements, so the benefit of NEFEM is not as high as before due to the selected global measure of the error, namely the $\mathcal{L}^2(\Omega)$ norm.

The last example considered is a Maltese cross (or Geneva drive) mechanism. This is imported, pre-processed and analysed following the steps outlined in Section 3 showing the ability to handle geometries that contain closed curves (i.e. the internal circle). The geometry, together with the computed Von Mises stress field, is shown in Fig. 9. This figure also shows a detailed view of the discretisation used near the boundary, highlighting the elements where the NEFEM formulation is used.

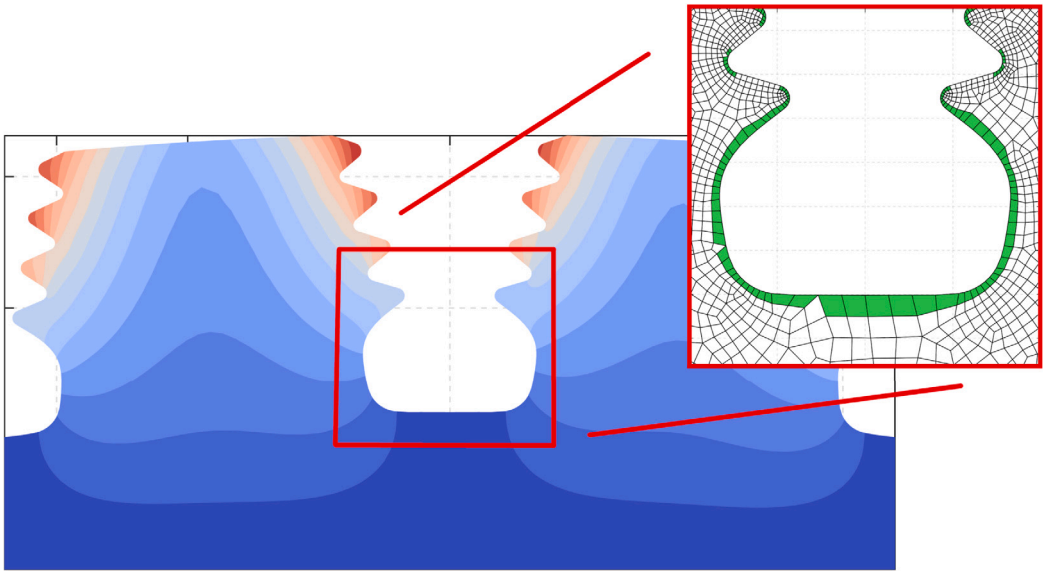

Fig. 8. Detailed view of the geometry of the fir tree and computed displacement field. A detailed view of the mesh near the boundary is also shown, highlighting the NEFEM (light green) and FEM (white) elements.

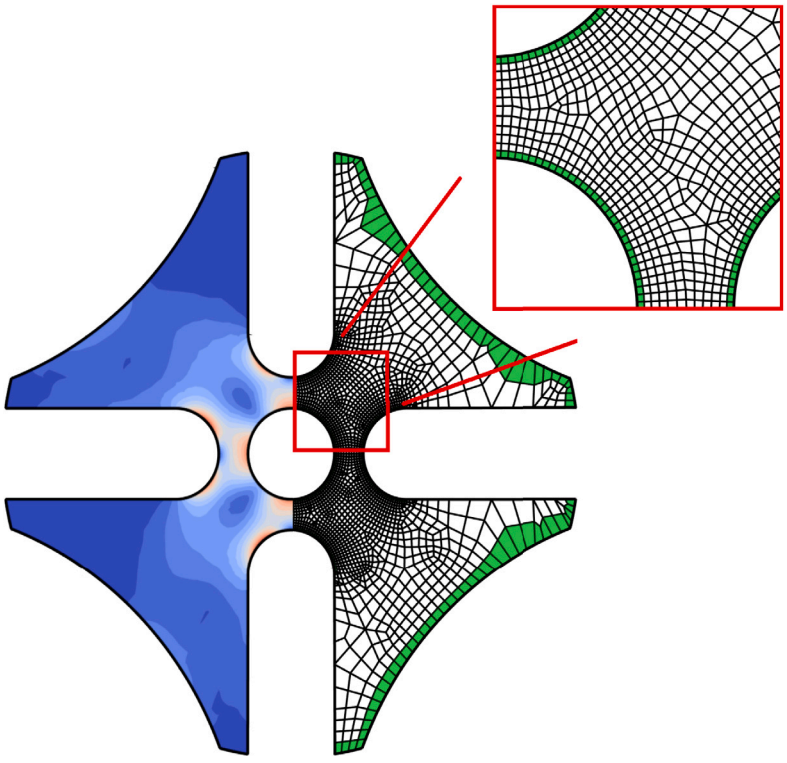

Fig. 9. Geometry of the Maltese cross and computed Von Mises stress field. A detailed view of the mesh near the boundary is also shown, highlighting the NEFEM (light green) and FEM (white) elements.

Homogeneous Dirichlet boundary conditions are applied on the inner circle part of the geometry and a rotational load is applied on all the straight edges of the four inserts. As no analytical solution is available for this problem, a reference solution, computed using bi-quadratic finite elements.

Table 4
Summary of the results for all the linear elastic problems presented in this paper.

	Number of elements			Error reduction
	FEM	NEFEM	Ratio	
Circular membrane (finest)	900	124	7.6:1	37.2%
Blade root	7897	606	13:1	12.8%
Maltese cross	3846	542	7:1	20.0%

The mesh contains 4388 quadrilateral elements and the preprocess stage partitions the mesh into 542 NEFEM elements and 3846 FEM elements. Computing the error of the FEM and NEFEM solutions, the results reveal that NEFEM is able to reduce the error by 20%. This again shows the potential of NFEEM even with a global measure of the error is considered.

We now present a study to assess what number of Gauss points produces results sufficiently accurate. The numerical quadrature described in Section 3.3.1 introduces an approximation that is proportional to the number of Gauss points used for the quadrature itself; the aim of this study is to provide an empirical rule of thumb which set a sufficient number of Gauss points. The idea is to start from a baseline value and measure the error as the number of Gauss points increases. The baseline is set to match the FEM formulation, which requires $p+1$ Gauss points for a shape function of order p: two Gauss points for each dimension of the parametric domain. This configuration gives a total error of 2.894. By increasing the number of Gauss points to nine, three for each direction, the error drops to 2.815. Numerical tests show that this value does not decrease significantly when adding more Gauss points and, since the error reached a plateau, we conclude that $p+2$ Gauss points are sufficient.

To conclude, Table 4 collects the results for the three linear elastic problems considered in this work, namely the Lamé problem considered in the previous section and the two problems involving more complex geometries analysed in this section.

It is clear that with the negligible extra cost introduced on boundary NEFEM elements, the proposed formulation is able to provide a significant reduction in the error for a given spatial discretisation. The improvement are related to the amount of curved elements and the complexity of the solution, but in all cases the incorporation of NEFEM elements is beneficial.

4.4. Discussion

The advantages and current limitations of the new quadrilateral element are presented in this section.
The new method offers:

1. Higher accuracy than FEM. This is demonstrated by a set of numerical examples involving heat transfer and linear elastic problems, including cases with complex geometries.
2. Seamless integration with current CAD. The new pre-processing algorithm was proven robust. It has also demonstrated ability to create NEFEM suitable models for complex CAD geometries and unstructured meshes.
3. Effective rule of thumb for numerical quadrature. Compared to standard FEM, only one extra Gauss point is required to produce accurate result.

The first advantage is essentially a consequence of the numerical integration strategy that accounts for the exact boundary representation. This results in a more accurate computation of both integrals in the boundary elements and integrals over edges on the boundary, required to impose the non-homogeneous natural conditions.

The second advantage is due to the direct use of the B-rep, without any further modification or transformation of the geometry that is naturally used by the CAD community.

The formulation proposed in this work brings the advantages of the NEFEM rationale for the first time to the finite element solid mechanics community. This is the first time NEFEM has been applied to quadrilateral elements and for solid mechanics problems solved using a traditional continuous Galerkin formulation. Despite that the formulation can be extended to other interpolation functions (e.g. Hermitian, bicubic, etc...) the focus of the present work is limited to low order approximations due to the shortcomings of current mesh generators already discussed in Section 1.

5. Conclusions

This work proposed a new super-parametric mapping for FEM that integrates into de-facto CAD solutions. In particular, a quadrilateral element for NEFEM is presented along with applications to heat transfer and solid mechanics. The new element provides exact boundary representation of the computational domain, as given by a CAD model. This means that strong legacy with in-service CAD and FEM analysis systems is retained.

The method partitions the mesh in two sets of FEM and NEFEM elements. For NEFEM elements a new mapping is defined between the reference element and the physical element, with at least one edge on the NURBS boundary, whereas standard FEM is used in the rest of the domain. The only extra cost associated to NEFEM elements is therefore related to the extra number of integration points to be used in order to account for the rational definition of NURBS. However, this extra cost is negligible because NEFEM elements represent a small portion of the total number of elements. In addition, the method only requires to increase the number of points in one direction of the quadrilateral element, the one associated to the NURBS boundary.

The resulting method has been applied to heat transfer and solid mechanics problems with analytical solution, demonstrating the optimal convergence properties as the mesh is refined. In addition, two applications in solid mechanics involving complex geometries have also been considered to show the potential of the proposed method. For each example the accuracy of NEFEM has been evaluated and compared against traditional bi-linear elements. It has been found that, for the same mesh, NEFEM offers an error reduction between 25% and 50% with respect to the FEM counterpart.

Future development should include: (i) *robust* pre-processing algorithm for 3D geometries, (ii) a methodology to feed back into CAD the simulation results following approaches such as [48], and (iii) analysis of large deformations with emphasis on stress distribution, convergence studies, orthotropic materials and other scenarios in which quadrilateral elements are known to improve convergence drastically [49].

CRediT authorship contribution statement

Mattia Montanari: Conceptualization, Funding acquisition, Methodology, Project administration. **Gian Maria Santi:** Data curation, Formal analysis, Investigation, Software, Validation, Visualization, Writing – original draft, Writing – review & editing. **Ruben Sevilla:** Conceptualization, Formal analysis, Investigation, Methodology, Supervision, Writing – review & editing. **Liverani Alfredo:** Funding acquisition, Project administration, Supervision. **Nik Petrinic:** Project administration.

Declaration of competing interest

The authors declare the following financial interests/personal relationships which may be considered as potential competing interests: Prof Nik Petrinic reports financial support was provided by Engineering and Physical Sciences Research Council.

Data availability

No data was used for the research described in the article.

Acknowledgements

The permission of Rolls-Royce to publish this paper is gratefully acknowledged. This research forms part of the Rolls-Royce led EPSRC Prosperity Partnership EP/S005072/1 entitled Strategic Partnership in Computational Science for Advanced Simulation and Modelling of Virtual Systems: ASiMoV.

References

[1] T. Hughes, J. Cottrell, Y. Bazilevs, Isogeometric analysis: CAD, finite elements, NURBS, exact geometry and mesh refinement, Comput. Methods Appl. Mech. Engrg. 194 (39–41) (2005) 4135–4195, http://dx.doi.org/10.1016/j.cma.2004.10.008.
[2] K.A. Johannessen, T. Kvamsdal, T. Dokken, Isogeometric analysis using LR B-splines, Comput. Methods Appl. Mech. Engrg. 269 (2014) 471–514, http://dx.doi.org/10.1016/j.cma.2013.09.014.
[3] A. Perduta, R. Putanowicz, Tools and techniques for building models for isogeometric analysis, Adv. Eng. Softw. 127 (2019) 70–81, http://dx.doi.org/10.1016/j.advengsoft.2018.10.008.
[4] R. Sevilla, S. Fernández-Méndez, A. Huerta, 3D NURBS-Enhanced Finite Element Method (NEFEM), Internat. J. Numer. Methods Engrg. 88 (2) (2011) 103–125, http://dx.doi.org/10.1002/nme.3164.
[5] R. Sevilla, S. Fernández-Méndez, A. Huerta, NURBS-enhanced finite element method for Euler equations, Internat. J. Numer. Methods Fluids 57 (9) (2008) 1051–1069, http://dx.doi.org/10.1002/fld.1711.
[6] R. Sevilla, A. Huerta, HDG-NEFEM with degree adaptivity for stokes flows, J. Sci. Comput. 77 (3) (2018) 1953–1980, http://dx.doi.org/10.1007/s10915-018-0657-2.
[7] E. Cohen, T. Martin, R.M. Kirby, T. Lyche, R.F. Riesenfeld, Analysis-aware modeling: Understanding quality considerations in modeling for isogeometric analysis, Comput. Methods Appl. Mech. Engrg. 199 (5) (2010) 334–356, http://dx.doi.org/10.1016/j.cma.2009.09.010.
[8] F. Patrizi, C. Manni, F. Pelosi, H. Speleers, Adaptive refinement with locally linearly independent LR B-splines: Theory and applications, Comput. Methods Appl. Mech. Engrg. 369 (2020) 113230, http://dx.doi.org/10.1016/j.cma.2020.113230.
[9] J.A. Cottrell, T.J.R. Hughes, Y. Bazilevs, Isogeometric Analysis: Toward Integration of CAD and FEA, John Wiley & Sons, 2009.
[10] M. Scott, X. Li, T. Sederberg, T. Hughes, Local refinement of analysis-suitable T-splines, Comput. Methods Appl. Mech. Engrg. 213–216 (2012) 206–222, http://dx.doi.org/10.1016/j.cma.2011.11.022.
[11] S. Shojaee, E. Izadpanah, N. Valizadeh, J. Kiendl, Free vibration analysis of thin plates by using a NURBS-based isogeometric approach, Finite Elem. Anal. Des. 61 (2012) 23–34, http://dx.doi.org/10.1016/j.finel.2012.06.005, URL https://www.sciencedirect.com/science/article/pii/S0168874X12001199.
[12] A. Qarariyah, F. Deng, T. Yang, Y. Liu, J. Deng, Isogeometric analysis on implicit domains using weighted extended PHT-splines, J. Comput. Appl. Math. 350 (2019) 353–371, http://dx.doi.org/10.1016/j.cam.2018.10.012.
[13] T. Dokken, V. Skytt, O. Barrowclough, Trivariate spline representations for computer aided design and additive manufacturing, Comput. Math. Appl. 78 (7) (2019) 2168–2182, http://dx.doi.org/10.1016/j.camwa.2018.08.017.
[14] L. Chen, G. Xu, S. Wang, Z. Shi, J. Huang, Constructing volumetric parameterization based on directed graph simplification of L1 polycube structure from complex shapes, Comput. Methods Appl. Mech. Engrg. 351 (2019) 422–440, http://dx.doi.org/10.1016/j.cma.2019.01.036.
[15] F. Patrizi, T. Dokken, Linear dependence of bivariate minimal support and locally refined B-Splines over LR-meshes, Comput. Aided Geom. Design 77 (2020) 101803, http://dx.doi.org/10.1016/j.cagd.2019.101803.
[16] M.-C. Hsu, C. Wang, A.J. Herrema, D. Schillinger, A. Ghoshal, Y. Bazilevs, An interactive geometry modeling and parametric design platform for isogeometric analysis, Comput. Math. Appl. 70 (7) (2015) 1481–1500, http://dx.doi.org/10.1016/j.camwa.2015.04.002.
[17] M. Montanari, L. Li, N. Petrinic, Isogeometric models for impact analysis with LS-DYNA, in: 11th European LS-DYNA Conference 2017, Salzburg, Austria, 2017.

[18] D. Kamensky, Y. Bazilevs, tIGAr: Automating isogeometric analysis with FEniCS, Comput. Methods Appl. Mech. Engrg. 344 (2019) 477–498, http://dx.doi.org/10.1016/j.cma.2018.10.002.
[19] T. Veldin, B. Brank, M. Brojan, Discrete Kirchhoff-Love shell quadrilateral finite element designed from cubic Hermite edge curves and Coons surface patch, Thin-Walled Struct. 168 (108268) (2021) 1–20, URL https://plus.cobiss.net/cobiss/si/en/bib/73890819.
[20] G. Xu, M. Li, B. Mourrain, T. Rabczuk, J. Xu, S.P.A. Bordas, Constructing IGA-suitable planar parameterization from complex CAD boundary by domain partition and global/local optimization, Comput. Methods Appl. Mech. Engrg. 328 (2018) 175–200, http://dx.doi.org/10.1016/j.cma.2017.08.052.
[21] G. Xu, B. Mourrain, A. Galligo, T. Rabczuk, High-quality construction of analysis-suitable trivariate NURBS solids by reparameterization methods, Comput. Mech. 54 (5) (2014) 1303–1313, http://dx.doi.org/10.1007/s00466-014-1060-y.
[22] D. Miao, Z. Zou, M.A. Scott, M.J. Borden, D.C. Thomas, Isogeometric Bézier dual mortaring: The enriched Bézier dual basis with application to second- and fourth-order problems, Comput. Methods Appl. Mech. Engrg. 363 (2020) 112900, http://dx.doi.org/10.1016/j.cma.2020.112900.
[23] L. Li, D. Benson, A. Nagy, M. Montanari, N. Petrinic, S. Hartmann, Recent developments in isogeometric analysis with solid elements in LS-DYNA®, in: Isogeometric Analysis, 2018, p. 10.
[24] J. Xie, J. Xu, Z. Dong, G. Xu, C. Deng, B. Mourrain, Y.J. Zhang, Interpolatory Catmull-Clark volumetric subdivision over unstructured hexahedral meshes for modeling and simulation applications, Comput. Aided Geom. Design 80 (2020) 101867, http://dx.doi.org/10.1016/j.cagd.2020.101867.
[25] S. Habib, C. Kezrane, B. Hachi, Moving local mesh based on analysis-suitable T-splines and Bézier extraction for extended isogeometric finite element analysis - Application to two-dimensional crack propagation, Finite Elem. Anal. Des. 213 (2023) 103854, http://dx.doi.org/10.1016/j.finel.2022.103854, URL https://www.sciencedirect.com/science/article/pii/S0168874X22001275.
[26] G. Xu, Y. Jin, Z. Xiao, Q. Wu, B. Mourrain, T. Rabczuk, Exact conversion from Bézier tetrahedra to Bézier hexahedra, Comput. Aided Geom. Design 62 (2018) 154–165, http://dx.doi.org/10.1016/j.cagd.2018.03.022.
[27] P. Kang, S.-K. Youn, Isogeometric analysis of topologically complex shell structures, Finite Elem. Anal. Des. 99 (2015) 68–81, http://dx.doi.org/10.1016/j.finel.2015.02.002, URL https://www.sciencedirect.com/science/article/pii/S0168874X15000141.
[28] P. Kang, S.-K. Youn, Isogeometric topology optimization of shell structures using trimmed NURBS surfaces, Finite Elem. Anal. Des. 120 (2016) 18–40, http://dx.doi.org/10.1016/j.finel.2016.06.003, URL https://www.sciencedirect.com/science/article/pii/S0168874X16300798.
[29] V.P. Nguyen, P. Kerfriden, S.P.A. Bordas, T. Rabczuk, Isogeometric analysis suitable trivariate NURBS representation of composite panels with a new offset algorithm, Comput. Aided Des. 55 (2014) 49–63, http://dx.doi.org/10.1016/j.cad.2014.05.004.
[30] M. Pan, F. Chen, W. Tong, Volumetric spline parameterization for isogeometric analysis, Comput. Methods Appl. Mech. Engrg. 359 (2020) 112769, http://dx.doi.org/10.1016/j.cma.2019.112769.
[31] A. Shamanskiy, M.H. Gfrerer, J. Hinz, B. Simeon, Isogeometric parametrization inspired by large elastic deformation, Comput. Methods Appl. Mech. Engrg. 363 (2020) 112920, http://dx.doi.org/10.1016/j.cma.2020.112920.
[32] J. Ge, B. Guo, G. Yang, Q. Sun, J. Lu, Blending isogeometric and Lagrangian elements in three-dimensional analysis, Finite Elem. Anal. Des. 112 (2016) 50–63, http://dx.doi.org/10.1016/j.finel.2015.12.009, URL https://www.sciencedirect.com/science/article/pii/S0168874X15001973.
[33] R. Sevilla, HDG-NEFEM for two dimensional linear elasticity, Comput. Struct. 220 (2019) 69–80, http://dx.doi.org/10.1016/j.compstruc.2019.05.005.
[34] X. Meng, G. Hu, A NURBS-enhanced finite volume solver for steady Euler equations, J. Comput. Phys. 359 (2018) 77–92, http://dx.doi.org/10.1016/j.jcp.2017.12.041, URL https://www.sciencedirect.com/science/article/pii/S002199911730935X.
[35] A. Stavrev, P. Knechtges, S. Elgeti, A. Huerta, Space-time NURBS-enhanced finite elements for free-surface flows in 2D, Int. J. Numer. Methods Fluids 81 (7) (2016) 426–450, http://dx.doi.org/10.1002/fld.4189.
[36] M. Make, N. Hosters, M. Behr, S. Elgeti, Space-Time NURBS-Enhanced Finite Elements for Solving the Compressible Navier–Stokes Equations, in: Lecture Notes in Computational Science and Engineering, vol. 132, 2020, pp. 97–107.
[37] S. Soghrati, R.A. Merel, NURBS enhanced HIFEM: A fully mesh-independent method with zero geometric discretization error, Finite Elem. Anal. Des. 120 (2016) 68–79, http://dx.doi.org/10.1016/j.finel.2016.06.007, URL https://www.sciencedirect.com/science/article/pii/S0168874X16301007.
[38] R. Sevilla, L. Rees, O. Hassan, The generation of triangular meshes for NURBS-enhanced FEM, Internat. J. Numer. Methods Engrg. 108 (8) (2016) 941–968, http://dx.doi.org/10.1002/nme.5247.
[39] G. Legrain, A NURBS enhanced extended finite element approach for unfitted CAD analysis, Comput. Mech. 1–17, http://dx.doi.org/10.1007/s00466-013-0854-7.
[40] Q. Wang, W. Zhou, Y. Cheng, G. Ma, X. Chang, NURBS-enhanced line integration boundary element method for 2D elasticity problems with body forces, Comput. Math. Appl. 77 (7) (2019) 2006–2028, http://dx.doi.org/10.1016/j.camwa.2018.11.039, URL http://www.sciencedirect.com/science/article/pii/S0898122118306928.
[41] R. Sevilla, E. Barbieri, NURBS distance fields for extremely curved cracks, Comput. Mech. 54 (6) (2014) 1431–1446, http://dx.doi.org/10.1007/s00466-014-1067-4.
[42] K.J. Bathe, Finite Element Procedures, Klaus-Jurgen Bathe, Boston, Mass., 2007.
[43] M. Safdari, A.R. Najafi, N.R. Sottos, P.H. Geubelle, A NURBS-based interface-enriched generalized finite element method for problems with complex discontinuous gradient fields, Internat. J. Numer. Methods Engrg. 101 (12) (2015) 950–964, http://dx.doi.org/10.1002/nme.4852, URL https://onlinelibrary.wiley.com/doi/10.1002/nme.4852.
[44] R. Sevilla, S. Fernández-Méndez, A. Huerta, Comparison of high-order curved finite elements, Internat. J. Numer. Methods Engrg. 87 (8) (2011) 719–734, http://dx.doi.org/10.1002/nme.3129.
[45] T. Hughes, A. Reali, G. Sangalli, Efficient quadrature for NURBS-based isogeometric analysis, Comput. Methods Appl. Mech. Engrg. 199 (5–8) (2010) 301–313, http://dx.doi.org/10.1016/j.cma.2008.12.004.
[46] T.J. Hughes, Isogeometric analysis: Introduction and overview, 2010.
[47] S.A. Coons, Surfaces for Computer-Aided Design of Space Forms, Technical Report, Massachusetts Institute of Technology, USA, 1967.
[48] J. López, C. Anitescu, T. Rabczuk, CAD-compatible structural shape optimization with a movable Bézier tetrahedral mesh, Comput. Methods Appl. Mech. Engrg. 367 (2020) 113066, http://dx.doi.org/10.1016/j.cma.2020.113066.
[49] O.C. Zienkiewicz, R.L. Taylor, J.Z. Zhu, The Finite Element Method: Its Basis and Fundamentals, Sixth Edition, sixth ed., Butterworth-Heinemann, 2005.